# Syntheses, Crystal Structures and Properties of Two New Zn Based Boron Imidazolate Frameworks①

BI Ming-Yue[a, b] WEN Yi-Hang[a②]
ZHANG Hai-Xia[b] ZHANG Jian[b]

[a] (*Zhejiang Key Laboratory for Reactive Chemistry on Solid Surfaces, Institute of Physical Chemistry, Zhejiang Normal University, Jinhua* 321004, *China*)

[b] (*State Key Laboratory of Structural Chemistry, Fujian Institute of Research on the Structure of Matter, Chinese Academy of Sciences, Fuzhou* 350002, *China*)

**ABSTRACT** Two new boron imidazolate frameworks (BIFs), $Zn_2[HBH(2\text{-}mim)_3]_2(1,2\text{-}PEA)_2(EG)_2$ (**BIF-120**, EG = ethylene glycol) and $Zn[BH(2\text{-}mim)_3](1,2\text{-}HPEA)$ (**BIF-121**), were successfully synthesized by mixing the $KBH(2\text{-}mim)_3$ ligand and the semirigid aromatic dicarboxylate ligand 1,2-benzenediacetic acid (1,2-$H_2$PEA) under solvothermal conditions. In this paper, the two samples were structurally characterized by single-crystal X-ray diffraction and tested by infrared spectroscopy (IR), UV-visible spectroscopy (UV-Vis), thermogravimetric analysis TGA and X-ray powder diffractions. In addition, the solid-state luminescent properties of these crystals were also investigated.

**Keywords: boron imidazolate frameworks, crystal structure, X-ray crystallography, luminescent;**
**DOI: 10.14102/j.cnki.0254–5861.2011–3068**

## 1 INTRODUCTION

Metal-organic frameworks (MOFs)[1-5] have attracted intensive attention because of their fascinating topological structures as well as their potential applications in gas storage/separation, catalysis, dye degradation, sensing, etc. Boron imidazolate frameworks (BIFs) are a sub-class of MOFs constructed by cross-linking various pre-synthesized boron imidazolate ligands and metal cations[6-15]. Due to the tetrahedral configuration of the boron imidazolate ligands, a number of BIF materials have been synthesized by simulating inorganic zeolite $AlPO_4$, such as SOD-type BIF-3[6], RHO-type BIF-9[8], ACO-type BIF-22[12], interrupted-LTA-type BIF-20[11], and interrupted-ATN-type BIF-21[11]. These structures possess high density of imidazolium functional groups and tetradentate metal centers on the pore surface. So, BIFs show unique advantages for potential applications in $CO_2$ capture and photocatalytic reduction reaction owing to the presence of functional pore surfaces[13-21]. Recent studies have revealed a number of BIFs that exhibit high performance in photocatalytic $CO_2$ reduction. In this context, the design and synthesis of new BIFs are quite desirable.

Due to only containing N-donor, the coordination mode of boron imidazolate ligands is limited. In order to construct diverse structures in BIFs, an effective strategy is to co-assemble with carboxylate ligands. To date, a variety of BIFs have been built based on mixing boron imidazolate ligands with long flexible carboxylate ligands or short rigid carboxylate ligands. However, the semirigid carboxylate as an auxiliary ligand used in the BIF system has not been reported. The introduction of semirigid ligand in BIF provides new opportunity for constructing unique structures. Here, two new BIFs were successfully synthesized by employing the $BH(2\text{-}mim)_3^-$ ligand and the semirigid aromatic dicarboxylate ligand 1,2-benzenediacetic acid (1,2-PEA) under solvothermal condition. Single-crystal X-ray diffraction analysis revealed that $Zn_2[HBH(2\text{-}mim)_3]_2(1,2\text{-}PEA)_2(EG)_2$ (**BIF-120**) and $Zn[BH(2\text{-}mim)_3](1,2\text{-}HPEA)$ (**BIF-121**) possess 2-dimentional layer frameworks. Moreover, the solid-state luminescent properties of these crystals were also investigated.

Received 13 December 2020; accepted 21 February 2021 (**CCDC 2049002 for BIF-120 and 2049003 for BIF-121)**

① We gratefully acknowledge the National Key Research and Development Program of China (No. 2018YFA0208600)

② Corresponding author. Wen Yi-Hang, E-mail: wyh@zjnu.cn

## 2 EXPERIMENTAL

### 2. 1 Materials and instruments

All reagents were purchased commercially and used without further purification. Powder X-ray diffraction analyses were recorded on a Rigaku Dmax2500 diffractometer with Cu$K\alpha$ radiation ($\lambda$ = 1.54056 Å) with a step size of 0.02°. Thermal stability studies were carried out on a NETSCHZ STA-449C thermoanalyzer at a heating rate of 10 K/min under a $N_2$ atmosphere. Photoluminescent spectra were measured using a fluorescent spectrophotometer (Edinburgh, FLS980). IR spectra (KBr pellets) were recorded on an ABB Bomem MB102 spectrometer over a range of 400～4000 $cm^{-1}$.

### 2. 2 Syntheses of BIF-120 and BIF-121

KBH $(2\text{-mim})_3$ (35 mg, 0.12 mmol), $Zn(CH_3COO)_2 \cdot 2H_2O$ (26 mg, 0.12 mmol) and 1,2-benzenediacetic acid (29 mg, 0.15 mmol) in a mixed solvent of isopropanol (1 mL)/ethylene glycol (2 mL)/water (2 mL) were placed in a 20 mL vial. After that, the sample was heated at 80 ℃ for 3 days and then cooled to room temperature. After filtration, the powder was washed with ethanol and distilled water to obtain colorless crystals (**BIF-120**) (36 mg, yield about 17%, calculated based on $Zn(CH_3COO)_2 \cdot 2H_2O$).

KBH $(2\text{-mim})_3$ (35 mg, 0.12 mmol), $Zn(CH_3COO)_2 \cdot 2H_2O$ (26 mg, 0.12 mmol) and 1,2-benzenediacetic acid (29 mg, 0.15 mmol) in a mixed solvent of *n*-propanol (1 mL)/DMSO (2 mL)/water (2 mL) were placed in a 20 mL vial. The sample was then heated at 80 ℃ for 3 days followed by cooling to room temperature. After filtration, the powder was washed with ethanol and distilled water to obtain colorless crystals (**BIF-121**) (30 mg, yield about 14%, calculated based on $Zn(CH_3COO)_2 \cdot 2H_2O$).

For IR, the KBr tablet method was used to prepare samples, and the data were normalized to find the characteristic peak of 13000～1500 $cm^{-1}$. The main characteristic peaks of BIF-120 are 3480, 2815, 1401, 1375, 1305, 1118 and 745 $cm^{-1}$, and those of BIF-121 are 3185, 2560, 1805, 1505, 1480, 1335, 1305, 1005 and 750 $cm^{-1}$.

### 2. 3 Crystal structure determination

Colorless crystals of **BIF-120** and **BIF-121** were selected for diffraction data collection on a ROD, Synergy Custom system, HyPix diffractometer. The crystal was kept at 108.33(10) K during data collection. Using Olex2, the structure was solved with the ShelXT structure solution program using Intrinsic Phasing and refined with the ShelXL refinement package using Least-Squares minimization. All atoms were refined with anisotropic thermal parameters.

Crystal data for **BIF-120** ($Zn_2[HBH(2\text{-mim})_3]_2(1,2\text{-PEA})_2(EG)_2$, $M$ = 1150.44 g/mol): monoclinic, space group $Cc$, $a$ = 19.4341(3), $b$ = 14.2818(2), $c$ = 20.4023(3) Å, $\beta$ = 110.933(2)°, $V$ = 5288.99(15) $Å^3$, $Z$ = 4, $T$ = 108.33(10) K, $\mu$(Ga$K\alpha$) = 1.066 $mm^{-1}$, $D_c$ = 1.445 $g/cm^3$, 28311 reflections measured (6.846°≤2$\theta$≤113.8°), 9018 unique ($R_{int}$ = 0.0338, $R_{sigma}$ = 0.0291) which were used in all calculations. The final $R$ = 0.0402 ($I > 2\sigma(I)$) and $wR$ = 0.1103 (all data).

Crystal data for **BIF-121** ($Zn[BH(2\text{-mim})_3](1,2\text{-HPEA})$, $M$ = 554.73 g/mol): orthorhombic, space group $Pbca$, $a$ = 15.6472(7), $b$ = 15.5892(8), $c$ = 21.1110(9) Å, $V$ = 5149.5(4) $Å^3$, $Z$ = 8, $T$ = 100.00(11) K, $\mu$(Cu$K\alpha$) = 1.686 $mm^{-1}$, $D_c$ = 1.431 $g/cm^3$, 15504 reflections measured (9.038°≤2$\theta$≤133.166°), 4232 unique ($R_{int}$ = 0.0331, $R_{sigma}$ = 0.0263) which were used in all calculations. The final $R$ = 0.0319 ($I > 2\sigma(I)$) and $wR$ = 0.0889 (all data).

## 3 RESULTS AND DISCUSSION

### 3. 1 Crystal structure descriptions of BIF-120 and BIF-121

Single-crystal X-ray structure analysis showed that **BIF-120** crystalizes in the monoclinic space group *Cc*. As shown in Fig. 1, the asymmetric unit contained two Zn ions, two $HBH(2\text{-mim})_3$ ligands and two 1,2-PEA ligands. Both of the Zn ions adopted a $ZnN_2O_2$ tetrahedral geometry. Each Zn ion was four-coordinated with two N atoms from two different $HBH(2\text{-mim})_3$ ligands and two O atoms from two different 1,2-PEA ligands. The tridentate $BH(2\text{-mim})_3^-$ ligands were protonated during the crystallization process. Two $HBH(2\text{-mim})_3$ ligands linked bridged two Zn ions to form a regular quadrilateron with the 2-methylimidazole ring as the four sides (Fig. 1). The Zn–N bond lengths range from 1.988 to 2.024 Å and the Zn–O bond lengths vary from 1.948 to 1.964 Å, respectively. Each B atom is covalently bound to three N atoms from 2-methylimidazole ligands with B–N bond lengths from 1.527 to 1.567 Å. Each 1,2-PEA ligand adopted a bis-monodentate coordination mode linking two adjacent regular quadrangles to form a 2-dimensional layer (Fig. 2a). As shown in Fig. 2b, the 2*D* layers packed with each other to generate a 3-dimensional supramolecule. Moreover, rich hydrogen bonding interactions exist between them and further stabilize the 3-dimensional framework of **BIF-120**.

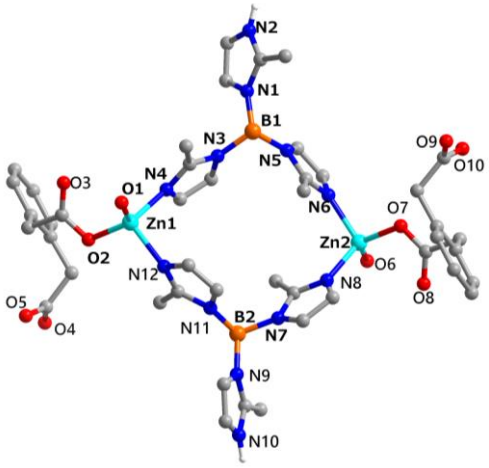


**Fig. 1. Coordination environment in BIF-120**

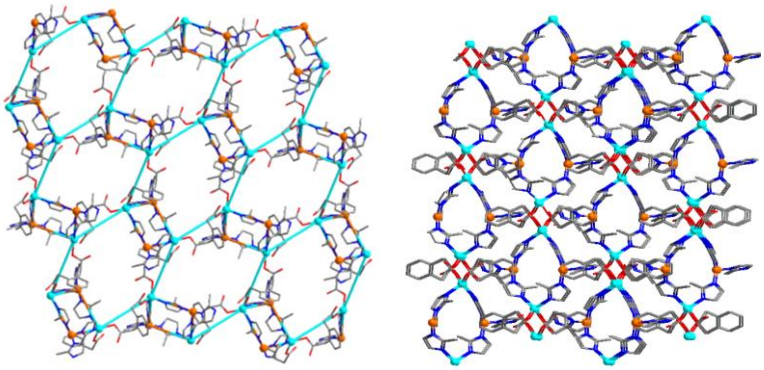

**(a)** **(b)**

**Fig. 2. (a) 2-dimensional layer in the *bc* plane; (b) 2*D* layer structure in BIF-120**

Single-crystal X-ray structure analysis showed that **BIF-121** crystalizes in the orthogonal space group *Pbca*. As shown in Fig. 3, the asymmetric unit contained one crystallographic Zn ion, one $BH(2\text{-}mim)_3^-$ ligand and one 1,2-HPEA ligand. Each Zn ion was four-coordinated with three N atoms from three different $BH(2\text{-}mim)_3^-$ ligands and O atoms from the 1,2-HPEA ligands. The tridentate $BH(2\text{-}mim)_3^-$ ligand worked as $\mu_3$-bridge to link three adjacent Zn ions, leading to a 3-connected 2-dimensional layer (Fig. 4a). The coordination mode of ligand 1,2-HPEA in **BIF-121** was different from that of **BIF-120**. Only one carboxyl group of 1,2-HPEA ligand deprotonated to coordinate with Zn ion, and the other carboxyl group without deprotonation formed rich hydrogen bonds with the adjacent carboxyl oxygen and nitrogen on the imidazolate ring (Fig. 4b and Table 1). By considering the B and Zn atoms as the 3-connected nodes, the framework can be topologically regarded as 3-connected *hcb* type plane. Furthermore, 1,2-HPEA ligands bridged adjacent 2-dimensional layers by these hydrogen bonds to form a 3-dimensional framework (Fig. 5).

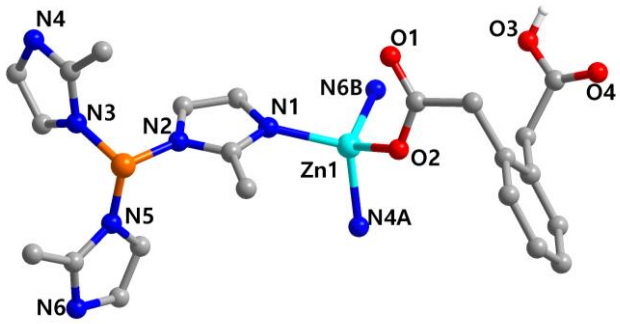


**Fig. 3. Coordination environment in BIF-121**

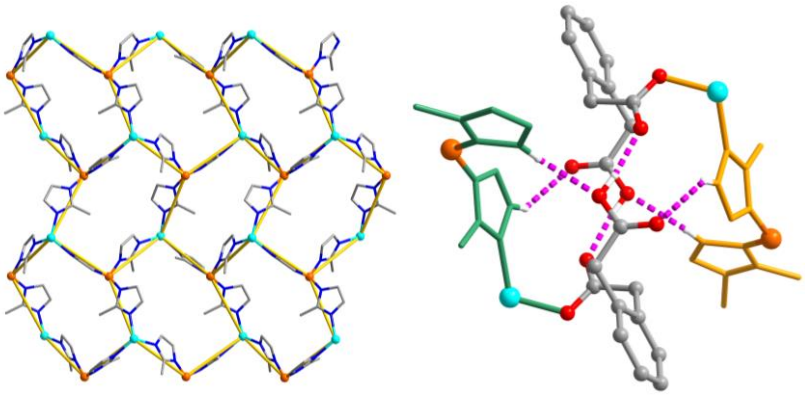

**(a)** **(b)**

**Fig. 4. (a) 2-dimensional layer in the *ac* plane; (b) Hydrogen bonding in BIF-121**

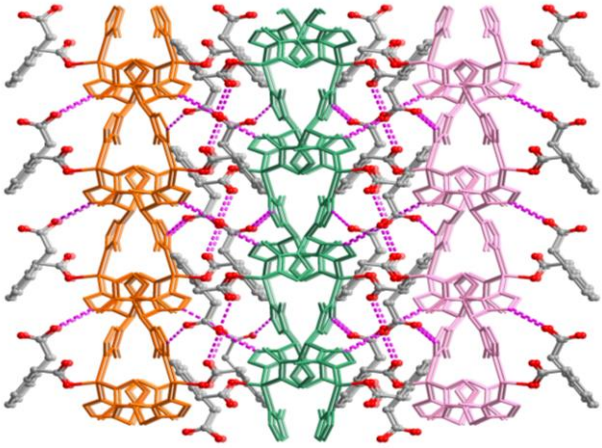

**Fig. 5. Packing motif of BIF-121**

**Table 1. Intermolecular Hydrogen Bonding Interactions (Å, °) in BIF-121**

| D–H | d(D–H) | d(H···A) | ∠DHA | d(D···A) | A |
|---|---|---|---|---|---|
| O(3)–H(3)$^{\#1}$ | 0.82 | 1.79 | 171 | 2.600(2) | O(1) |
| C(15)–H(15)$^{\#2}$ | 0.93 | 2.44 | 160 | 3.326(3) | O(3) |
| C(20)–H(20)$^{\#3}$ | 0.93 | 2.48 | 138 | 3.228(3) | O(4) |

Symmetry codes: #1: $-x+1, -y+2, -z+1$; #2: $-x+1, y-1/2, -z+1/2$; #3: $x, -y+3/2, z-1/2$

### 3. 2 Characterization of BIF-120 and BIF-121

The phase purity of the bulk samples of **BIF-120** and **BIF-121** was checked by powder X-ray diffraction (PXRD) patterns. As shown in Figs. S1 and S2**,** the XRD patterns of **BIF-120** and **BIF-121** were very consistent with the simulated patterns calculated from the single-crystal diffraction data, indicating the successful preparation and phase purity. Thermogravimetric analysis (TGA) in a $N_2$ atmosphere was studied to investigate the thermal stability. As indicated by the TGA data of **BIF-120** (Fig. S3), there was some weight loss of small guest molecules from room temperature to 100 ℃. It was stable up to 180 ℃, and finally the framework collapsed during heating. **BIF-121** (Fig. S5) had almost no weight loss above 250 ℃, which proves that **BIF-121** is more stable than **BIF-120**. But after three days of soaking in ethanol solution, the guest was exchanged. In Fig. S4, it can be seen that **BIF-120** is very stable below 180 ℃. The FTIR spectrum in Figs. S6 and S7 shows that the strong peaks of $v_{as}$ (-COO-) at 1500～1490 $cm^{-1}$ and $v_s$(-COO-) at 1350～1490 $cm^{-1}$ are assigned to the ligand 1,2-PEA carboxylic acid groups asymmetric and symmetric stretching vibration[22]. **BIF-120** and **BIF-121** were immersed in different solvents and different pH solutions for one day (Figs. S8 and S9), and compared with XRD after washing with ethanol. Both of them had better stability.

### 3. 3 Photoluminescence properties

From the perspective of the interaction between metal and ligand, an inorganic-organic hybrid coordination polymer composed of $\pi$-conjugated organic ligands 1,2-PEA and $d^{10}$ metal Zn(II) centers with photoluminescence properties[23, 24].

The fluorescence properties of complexes **BIF-120** and **BIF-121** have been tested in the solid state with 365 nm excitation light at room temperature (Fig. 6). It can be seen from the emission spectra that **BIF-120** shows a broad emission band at 425 nm and **BIF-121** shows it at 440 nm ($\lambda_{ex}$ = 365 nm), which may be attributed to the coordination interaction between the ligand and the central metal Zn(II)[25]. Compared with the free 1,2-PEA and KBH(2-mim)$_3$ ligands, **BIF-121** has a wide emission range, with a maximum peak at 440 nm, which has a red shift. This emission band can be temporarily attributed to the ligand-to-metal charge transfer (LMCT).

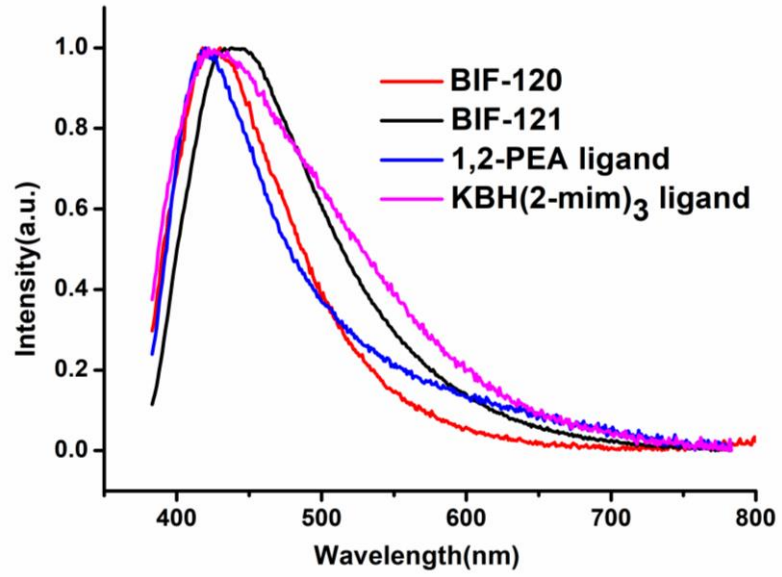


**Fig. 6. Emission spectra of BIF-120, BIF-121, 1,2-PEA and KBH(2-mim)$_3$ ligand ($\lambda_{ex}$ = 365 nm) in the solid state at room temperature**

## 4 CONCLUSION

In summary, two novel 2-dimensional boron imidazolate frameworks (**BIF-120** and **BIF-121**) with BH(mim)$_3^-$ and 1,2-benzenediacetic acids were successfully prepared and characterized by single-crystal X-ray diffraction analysis as well as spectroscopy. Solid-state photoluminescence studies revealed that **BIF-121** shows emission at 440 nm while **BIF-120** shows emission at 425 nm.

## REFERENCES

(1) Rouffet, M.; de Oliveira, C. A. F.; Udi, Y.; Agrawal, A.; Sagi, I.; McCammon, J. A.; Cohen, S. M. From sensors to silencers: quinoline- and benzimidazole-sulfonamides as inhibitors for zinc proteases. *J. Am. Chem. Soc*. **2010**, 132, 8232–8233.

(2) Xue, F.; Kumar, P.; Xu, W.; Mkhoyan, K. A.; Tsapatsis, M. Direct synthesis of 7 nm-thick zinc(II)-benzimidazole-acetate metal-organic framework nanosheets. *Chem. Mater*. **2017**, 30, 69–73.

(3) Combs, A. P.; Zhu, W.; Crawley, M. L.; Glass, B.; Polam, P.; Sparks, R. B.; Metcalf, B. Potent benzimidazole sulfonamide protein tyrosine phosphatase 1B inhibitors containing the heterocyclic (S)-isothiazolidinone phosphotyrosine mimetic. *J. Med. Chem*. **2006**, 49, 3774–3789.

(4) Chen, L. Z.; Ji, Q.; Dan, Y. Y. Synthesis, structure, and luminescent and dielectric properties of two novel 1*D* chains based on a T-shaped tripodal ligand 4-(4,5-dicarboxy-imidazol-2-yl)pyridine loxide. *Chin. J. Struct. Chem*. **2016**, 35, 1728–1735.

(5) Chen, L. Z.; Sun, J.; Ji, Q.; Pan, Q. J.; Huang, Y. Switchable dielectric materials based on 2-methylimidazole. *Chin. J. Struct. Chem*. **2017**, 36, 329–337.

(6) Zhang, J.; Wu, T.; Zhou, C.; Chen, S. M.; Feng, P. Y.; Bu, X. H. Zeolitic boron imidazolate frameworks. *Angew. Chem. Int. Ed*. **2009**, 48, 2580–2583.

(7) Zhang, H. X.; Liu, M.; Wen, T.; Zhang, J. Synthetic design of functional boron imidazolate frameworks. *Coord. Chem. Rev*. **2016**, 307, 255–266.

(8) Wu, T.; Zhang, J.; Zhou, C.; Wang, L.; Bu, X. H.; Feng, P. Y. Zeolite RHO-type net with the lightest elements. *J. Am. Chem. Soc.* **2009**, 131, 6111–6113.

(9) Zheng, S. T.; Wu, T.; Zhang, J.; Mina, C.; Nieto, R. A.; Bu, X. H.; Feng, P. Y. Porous metal carboxylate boron imidazolate frameworks. *Angew. Chem. Int. Ed*. **2010**, 49, 5362–5366.

(10) Wu, T.; Zhang, J.; Bu, X. H.; Feng, P. Y. Variable lithium coordination modes in two- and three-dimensional lithium boron imidazolate frameworks. *Chem. Mater*. **2009**, 21, 3830–3837.

(11) Zhang, H. X.; Wang, F.; Yang, H.; Tan, Y. X.; Zhang, J.; Bu, X. H. Interrupted zeolite LTA and ATN-type boron imidazolate frameworks. *J. Am. Chem. Soc.* **2011**, 133, 11884–11887.

(12) Wang, F.; Shu, Y. B.; Bu, X. H.; Zhang, J. Zeolitic boron imidazolate frameworks with 4-connected octahedral metal centers. *Chem. Eur. J*. **2012**, 18, 11876–11879.

(13) Gao, C.; Wang, J.; Xu, H. X.; Xiong, Y. J. Coordination chemistry in the design of heterogeneous photocatalyst. *Chem. Soc. Rev*. **2017**, 46, 2799–2823.

(14) Xu, G. L.; Zhang, H. B.; Wei, J.; Zhang, H. X.; Wu, X.; Li, Y.; Li, C. S.; Zhang, J.; Ye, J. H. Integrating the *g*-$C_3N_4$ nanosheet with B–H bonding decorated metal-organic framework for $CO_2$ activation and photoreduction. *ACS Nano*. **2018**, 12, 6, 5333–5340.

(15) Wang, S. B.; Yao, W. S.; Lin, J. L.; Ding, Z. X.; Wang, X. C. Cobalt imidazolate metal-organic frameworks photosplit $CO_2$ under mild reaction conditions. *Angew. Chem. Int. Ed*. **2014**, 53, 1034–1038.

(16) Zhang, T.; Lin, W. B. Metal-organic frameworks for artificial photosynthesis and photocatalysis. *Chem. Soc. Rev*. **2014**, 43, 5982–5993.

(17) Wang, Y.; Huang, N. Y.; Shen, J. Q.; Liao, P. Q.; Chen, X. M.; Zhang, J. P. Hydroxide ligands cooperate with catalytic centers in metal-organic frameworks for efficient photocatalytic $CO_2$ reduction. *J. Am. Chem. Soc.* **2017**, 38–41.

(18) Takeda, H.; Cometto, C.; Ishitani, O.; Robert, M. Photons, protons and earth-abundant metal complexes for molecular catalysis of $CO_2$ reduction. *ACS Catal*. **2017**, 7, 70–88.

(19) Liu, Q.; Low, Z. X.; Li, L.; Razmjou, A.; Wang, K.; Yao, J. F.; Wang, H. T. ZIF-8/$Zn_2GeO_4$ nanorods with an enhanced $CO_2$ adsorption property in an aqueous medium for photocatalytic synthesis of liquid fuel. *J. Mater. Chem. A* **2013**, 1, 11563–11569.

(20) Wang, Y.; Zhang, Z. Z.; Li, C.; Zhang, L. N.; Luo, Z. B.; Shen, J. N.; Lin, H. X.; Long, J. L.; Wu, J. C. S.; Fu, X. Z.; Wang, X. X. Visible-light driven overall conversion of $CO_2$ and $H_2O$ to $CH_4$ and $O_2$ on 3*D*-SiC@2*D*-$MoS_2$ heterostructure. *J. Am. Chem. Soc*. **2018**, 140, 14595–14598.

(21) Zhou, M.; Wang, S. B.; Yang, P. J.; Huang, C. J.; Wang, X. C. Boron carbon nitride semiconductors decorated with CdS nanoparticles for photocatalytic reduction of $CO_2$. *ACS Catal*. **2018**, 8, 4928–4936.

(22) Loiseau, T.; Serre, C.; Huguenard, C.; Fink, G.; Taulelle, F.; Henry, M.; Bataille, T.; Ferey, G. A rationale for the large breathing of the porous aluminum terephthalate (MIL-53) upon hydration. *Chem. Eur. J*. **2004**, 10, 1373–1382.

(23) Ma, L. F.; Wang, L. Y.; Hu, J. L.; Wang, Y. Y. Syntheses, structures, and photoluminescence of a series of $d^{10}$ coordination polymers with R-isophthalate (R = -OH, -$CH_3$, and -$C(CH_3)_3$). *Cryst. Growth Des*. **2009**, 9, 5334–5342.

(24) Han, M. L.; Chang, X. H.; Feng, X.; Ma, L. F.; Wang, L. Y. Temperature and pH driven self-assembly of Zn(II) coordination polymers: crystal structures, supramolecular isomerism, and photoluminescence. *CrystEngComm*. **2014**, 16, 1687–1695.

(25) Zhang, L. Y.; Zhang, J. P.; Lin, Y. Y.; Chen, X. M. Syntheses, structures, and photoluminescence of three coordination polymers of cadmium dicarboxylates. *Cryst. Growth Des*. **2006**, 6, 1684–1689.

(26) Dolomanov, O. V.; Bourhis, L. J.; Gildea, R. J.; Howarda, J. A. K.; Puschmann, K. OLEX2: a complete structure solution, refinement and analysis program. *J. Appl. Cryst.* **2009**, 42, 339–341.

(27) Dolomanov, O. V.; Puschmann, H. Accurate hydrogen-atom positions from standard X-ray data: Hirshfeld atom refinement and Olex2. *Acta Crystallogr A* **2018**, 74, e40–e40.